

Simulating the XANES of metalloenzymes – a case study

Ana Mijovilovich and Wolfram Meyer-Klaucke*

EMBL c/o DESY, Notkestrasse 85, Geb 25A, 22607 Hamburg, Germany. E-mail: wolfram@embl-hamburg.de

The analysis of XANES patterns is very indicative for screening samples. Powerful X-ray absorption spectroscopy data-analysis programs can simulate these patterns. Here, a case study on two structural motifs is presented: a non-heme Fe site (2-His-1-carboxylate motif) and the metallo β -lactamase dinuclear Zn site. Simulations of the edge shapes for different structural models will be compared with experimental results, pointing out limitations and challenges. The influence of single neighbouring atoms in the first and second shell on the resulting XANES pattern is discussed. Insights into catalytic mechanisms and the requirements for future theory development are addressed.

Keywords: XANES; simulation; enzyme; X-ray absorption spectroscopy (XAS).

1. Introduction

EXAFS provides structural information about the moiety of metal centres up to a distance of approximately 4–5 Å. Very accurate metal–ligand distances can be obtained for at least the first shell. For higher shells, the information available depends on the presence of overlapping contributions (Mijovilovich & Meyer-Klaucke, 2001). In the XANES region of an XAS (X-ray absorption spectroscopy) spectrum, the long lifetime of the photoelectron at low energies results in a long mean free path with contributions from atoms at higher distances. For solid crystalline materials, good convergence for the XANES simulation is frequently achieved with clusters of around 100 atoms and/or 10 Å radius (Ankudinov *et al.*, 1998). Catalytic active metal centres in enzymes are usually located in so-called ‘pockets’ surrounded by hydrophobic ligands. In contrast to crystalline solids, there is less long-range order (or long-range conserved symmetry) in proteins. Thus the simulations should converge for smaller clusters in the case of enzymes.

Moreover, at the low energies involved in XANES analysis, the influence of the Debye–Waller parameter is neglected. Therefore simulations might help to overcome the restrictions in EXAFS caused by the correlation between coordination number and Debye–Waller parameter. Finally, this could allow the determination of coordination numbers with higher accuracy.

Several codes are available to simulate the XANES profile. Depending on the author’s objective, they differ in their features. Some are extensions or upgrades of existing EXAFS refinement programs like *FEFF* (Ankudinov *et al.*, 1998) and *Excurve* (Strange *et al.*, 1990); others implement special features like the calculation of non-spherical potentials (Joly, 2001) or the refinement of inelastic losses and white-line intensity (Della Longa *et al.*, 2001). Here *FEFF8.10* is applied using full multiple scattering.

In this study we focus on two structural motifs: the mononuclear 2-His-1-carboxylate motif shared by many non-heme Fe enzymes and the dinuclear Zn β -lactamase motif.

The 2-His-1-carboxylate motif has been identified in a number of non-heme Fe enzymes, like extradiol cleaving catechol dioxygenases, Rieske dioxygenases, β -lactam antibiotic synthases and pterin-

dependent hydroxylases. It comprises one metal ion, typically Fe, and five or six O/N ligands, including two histidines and one carboxylate bound in a monodentate fashion. The remaining O atoms frequently belong to water molecules or OH groups (Que, 2000).

Many aspects of the catalytic activity are still not fully understood. Spectroscopic methods might help to elucidate subtle differences among different enzymes and species. In this contribution, we use XANES simulations as a new tool, addressing the following questions:

(i) Crystallographic data can be affected by photoreduction during data acquisition. Can XANES simulations characterize the metal oxidation state of a given crystal structure?

(ii) Frequently the coordination number and its change play a key role in understanding the catalytic mechanism. How does the coordination number affect the XANES?

(iii) Catechols like dopamine bind bidentate to human phenylalanine hydroxylase and replace two water molecules (Erlandsen *et al.*, 1998). Interestingly, the XANES reported for phenylalanine hydroxylase reduced by peroxide or dopamine is identical. Can this be understood on the basis of an XANES analysis?

(iv) Binding of pterin to the human enzyme (Erlandsen *et al.*, 2000) or treatment of the rat enzymes with either biopterin or phenylalanine (Loeb *et al.*, 1997) does not alter the six-coordination. Enzymes treated with both cofactor biopterin and substrate phenylalanine appear five-coordinated in MCD studies (Kemsley *et al.*, 1999). At present, there are no crystal structures available. How does the binding of cofactor and substrate affect metal moiety? Is it possible to determine the ligand removed?

For reasons that will be discussed later, the first example presents a rather ideal case for the XANES programs available at present. A more advanced case is represented by proteins of the metallo β -lactamase family, mostly comprising a dinuclear Zn-atom site. The name-giving members of this family provide bacterial resistance to β -lactam antibiotics. Enzymes with a β -lactamase motif include three histidines and one bridging water for the first metal site, called the 3H site. The second site (DCH site) is composed of five ligands: the bridging water, aspartate, cysteine or a further aspartate, histidine, and a terminal water. Both metals are bridged by either a water molecule or a monodentate carboxylate group. Again, we investigated whether XANES simulations can provide insight into several points:

(i) Several metallo β -lactamases exhibit full activity with only one Zn atom bound. Can XANES analysis locate a single Zn atom at the active site?

(ii) To what extent does binding of the second Zn atom alter the simulations generated for each site? Experimental XANES on mono- and dinuclear Zn β -lactamases show surprisingly little difference (De Seny *et al.*, 2001).

(iii) The cysteine present at the DCH site is not conserved for all metallo β -lactamases (Hernandez-Valladares *et al.*, 2000). To study its influence on the XANES pattern, the high-resolution crystal structure of human glyoxalase II (Cameron *et al.*, 1999) was taken as a model system; here cysteine is replaced by an aspartate residue.

The spatial arrangement of the ligands strongly influences the XANES pattern. Recently, it was reported by Penner-Hahn (2000) that different structures might exhibit similar XANES patterns. The possibility of multiple solutions will therefore be briefly discussed.

2. Methods

Simulations were performed with the program *FEFF8.10* (Ankudinov *et al.*, 1998). The *K*-edge XANES spectra were calculated using

self-consistent-field muffin-tin potentials with 15% overlap. The angular momentum l_{\max} was set to the maximum atomic momentum of the central atom. The Hedin–Lundqvist exchange-correlation potential for the excited state gave the best results. Extrinsic losses due to the propagation of the photoelectron are included in the self-energy. Intrinsic losses (core-hole lifetime and experimental broadening effects) can be included by convolution with a Lorentzian. The code offers the option of calculating the overlap integral S_0^2 in the presence of a fully relaxed core hole, but we found the correction too small. Therefore, only a small imaginary part (0.5 eV) was included to account for the experimental broadening. For the ground state, the von Barth–Hedin exchange-correlation potential was used to calculate the atomic background μ_0 . *FEFF8.10* calculates spherical potentials. For the first test case, this is quite accurate. In a dinuclear enzyme with N/O and S ligands this is a crude estimate. Therefore it is important to check the results for such cases, since this estimation is used for most XANES programs available today.

Depending on the oxidation state and sample treatment, human tyrosine hydroxylase exhibits three distinct XANES patterns (Meyer-Klaucke *et al.*, 1996; Schünemann *et al.*, 1999): first the six-coordinated Fe(II) states, second the five-coordinated Fe(II) states and third the six-coordinated Fe(III) states. In order to simulate these patterns, the crystal structure of a 2-His-1-carboxylate family member with good resolution at the metal site is needed. For human phenylalanine hydroxylase, Erlandsen *et al.* (1997) report for the native enzyme at 2.0 Å resolution a six-coordinated Fe ion, which is consistent with all spectroscopic results. Therefore most simulations are based on this model. For comparison, the structure of tyrosine hydroxylase (2.3 Å) that differs in the orientation of the glutamate group (Goodwill *et al.*, 1997) is used. Both structures report metal–ligand distances that are longer than those determined by EXAFS. The later distances agree with the typical distances reported for small molecules. Thus, in both cases, the metal–ligand distances were corrected to match the first-shell distance obtained by EXAFS for each oxidation state (Mijovilovich *et al.*, 2003). This can be achieved by moving the whole ligand or by multiplying the structure by a compression factor. Modifications in the first shell proved to be more important than the errors introduced in higher shells when multiplied by a compression factor. Thus the second approach was chosen because of its simplicity.

High qualitative similarity with the experimental results is obtained with a cluster including 19 atoms within a radius of 4.33 Å and 4.12 Å for Fe(II) and Fe(III), respectively (Fig. 1). Up to these distances, the contributing atoms are those associated with the first-shell ligands and one O atom from the residue Glu286. Using a cluster of 30 atoms that also includes contributions of the residues Tyr325, Ala345, Pro281, Phe263 and Glu286 (Fig. 1, in grey) gives rise to a shoulder at 7131 eV that is not present in the experimental data (see Fig. 2c). This might be due to artificial charge densities introduced in the calculation of the muffin-tin potentials. It is very likely that the contributions of such non-ligating residues average out due to static disorder over a huge number of metal sites. This static disorder is not considered by the method, therefore we neglect the non-ligated residues.

A small charge corresponding to one-fifth of the valence was introduced for the central Fe to increase the simulated white-line intensity. Because the muffin-tin potential lacks non-spherical corrections, the intensities of the white lines do not fully match the experimental data. No energy shift of the edge position was introduced.

Several XANES spectra for metallo β -lactamases are reported. Here we refer to those of *Bacillus cereus* II (Feiters, 1990; Meyer-

Klaucke *et al.*, 1999), for which crystal structures are available. Identical metal sites are identified at higher resolution (1.85 Å) for *Bacteroides fragilis* [PDB code 1ZNB (Carfi *et al.*, 1998)], which is used in this study. For human glyoxalase II, where the cysteine of the DCH site is replaced by an aspartate, a high-resolution structure (1.9 Å) is available as well [PDB code 1QH3 (Cameron *et al.*, 1999)]. The later structure includes a cacodylate, which was neglected in our calculations. The first ligands for each metal site were included in the calculations. For *Bacteroides fragilis*, Cys181, His223, Asp103 and two water molecules (one of them bridging both metals) for the DCH site and His162, His101, His99 and the bridging water molecule for the 3H site were considered (Fig. 3). For glyoxalase II, the ligands for the DCH site were Asp134, one bridging water molecule, His173, His59 and Asp58, and for the 3H site one bridging water molecule, Asp134, His110, His54 and His56 were taken into account. Introducing the O ion of the cacodylate into both the DCH and the 3H sites does not generate new features, but increases the intensity of the white line, as expected when increasing the coordination number (from five to six for both sites). Again distances were corrected for EXAFS results. The edge positions for the Zn *K*-edge had to be shifted by -9.0 eV for the 3H and -5.0 eV for the DCH site.

3. Results

3.1. '2-His-1-carboxylate' motif

The XANES patterns reported for the 2-His-1-carboxylate motif form three distinct groups: six-coordinated Fe(II) states, five-coordinated Fe(II) states and six-coordinated Fe(III) states. Fig. 2(a) displays these edge shapes for human tyrosine hydroxylase (Meyer-Klaucke *et al.*, 1996; Schünemann *et al.*, 1999). Similar patterns are measured for the six-coordinated states of phenylalanine hydroxylase (Mijovilovich *et al.*, 2003). How do simulations based on protein crystallography results fit the experimental XANES? The XANES profile generated on the basis of the phenylalanine hydroxylase structure resembles a mixture of both six-coordinated states, which suggests an occupation of about 50% for each individual oxidation state. This behaviour can either be caused by photoreduction during data collection or be due to a lack of resolution, because in protein crystallography the metal–ligand distance that is determined decreases with increasing resolution. EXAFS (Meyer-Klaucke *et al.*, 1996; Mijovilovich *et al.*, 2003; Loeb *et al.*, 1997) determines a shorter first-shell distance. Shrinking the metal moiety by a factor of 0.99 for Fe(II) and 0.94 for Fe(III) results in a structural model that is compatible with EXAFS. With these factors, the XANES calculations resemble the two experimental spectra (Fig. 2b).

In five-coordinated tyrosine hydroxylase, generated by lyophilization of the enzyme (Schünemann *et al.*, 1999), one of the water molecules is probably missing. This can be either the opposite of a histidine (water 426/water 427) or the carboxylate (water 428) (see Fig. 1). The multiple scattering within the first shell *via* the central metal ion provides two distinguished edge shapes. The simulation of five-coordinated tyrosine hydroxylase depends on the water molecule removed. The absence of water 426 causes the lowest white-line intensity while keeping all other edge features similar to those of the native enzyme. This behaviour is also seen in the experimental XANES data. In the crystal structure of tyrosine hydroxylase (Goodwill *et al.*, 1997) this water molecule is missing, most likely owing to the lack of resolution (2.3 Å) and a high Debye–Waller or temperature factor. Thus, both techniques agree on the low binding constant of this particular water molecule. It is probable that this water is removed in an initial phase of the catalytic cycle (Flatmark & Stevens, 1999).

Binding of substrate and cofactor to the active site of a metallo-enzyme frequently alters the shape of the XANES. For the 2-His-1-carboxylate family this is not the case; the small differences found were assigned to an incomplete reduction (Meyer-Klaucke *et al.*, 1996). Highlighting subtle differences based on simulations might be of assistance in future. The XANES patterns for the native state and for the state with either substrate or cofactor bound look very similar (not shown). This explains the lack of differences reported in the measurements. Difference spectra might be a way of handling such cases. Therefore, fully reduced samples and a very accurate energy calibration will play a key role.

3.2. β -Lactamase motif

The XANES of Zn β -lactamases exhibit patterns with several resonances. The spectra result from the superposition of two contributions: Zn_A bound to the 3H site and Zn_B present at the DCH site. Considering the limitations discussed in §3.1, we focus first on the 3H site. Protein crystallography and EXAFS have provided a structural model for this site (De Seny *et al.*, 2001; Carfi *et al.*, 1998). One of the remaining questions is the Zn_A–water distance. Simulations for various Zn_A–water distances at constant Zn_A–His₃ distances (Fig. 4b) point out the need for strong distortions to generate multiple resonances in the XANES region. On this basis, either a very short or a very long Zn_A–water distance is likely. Interestingly, this is consistent with recent EXAFS results (De Seny *et al.*, 2001).

The similarities found define a starting point for tackling the questions raised in §1 for the 3H site. As pointed out in §2, the ligands of both Zn-atom sites are considered for full simulations of the edge shape. For the edge pattern generated by Zn_A, it makes hardly any difference whether Zn_B is present or not (Fig. 4c).

In addition, simulations for the DCH site were calculated in the presence and absence of Zn_A. Again the contribution of the second metal is hardly recognized. This is consistent with reports on the XANES of half- and fully-metal-loaded β -lactamase (Meyer-Klaucke *et al.*, 1999).

The cysteine ligand of Zn_B plays a key role in the catalytic mechanism (Paul-Soto *et al.*, 1999). In order to study its effect on the XANES pattern generated by Zn_B, glyoxalase II was chosen as a model system (Cameron *et al.*, 1999), having an aspartate ligand

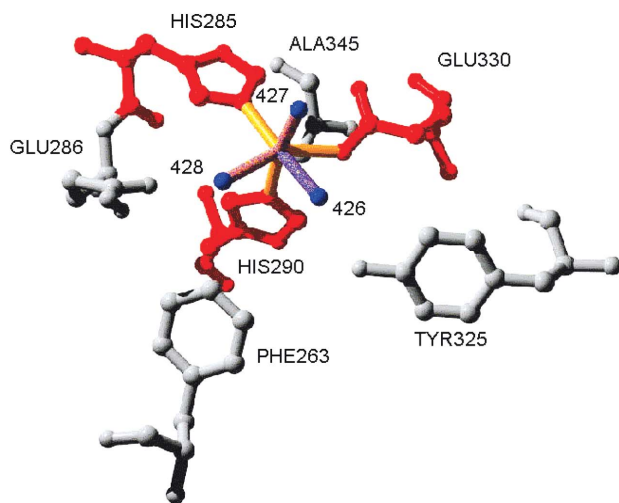


Figure 1

The 2-His-1-carboxylate motif in human phenylalanine hydroxylase. Metal ligands are depicted in red, and further residues close to the active site are depicted in grey.

instead of the cysteine. The presence of sulfur diminishes the white-line intensity and the depth of the first minimum, which is consistent with reports on model systems (Clark-Baldwin *et al.*, 1998; Jacquamet

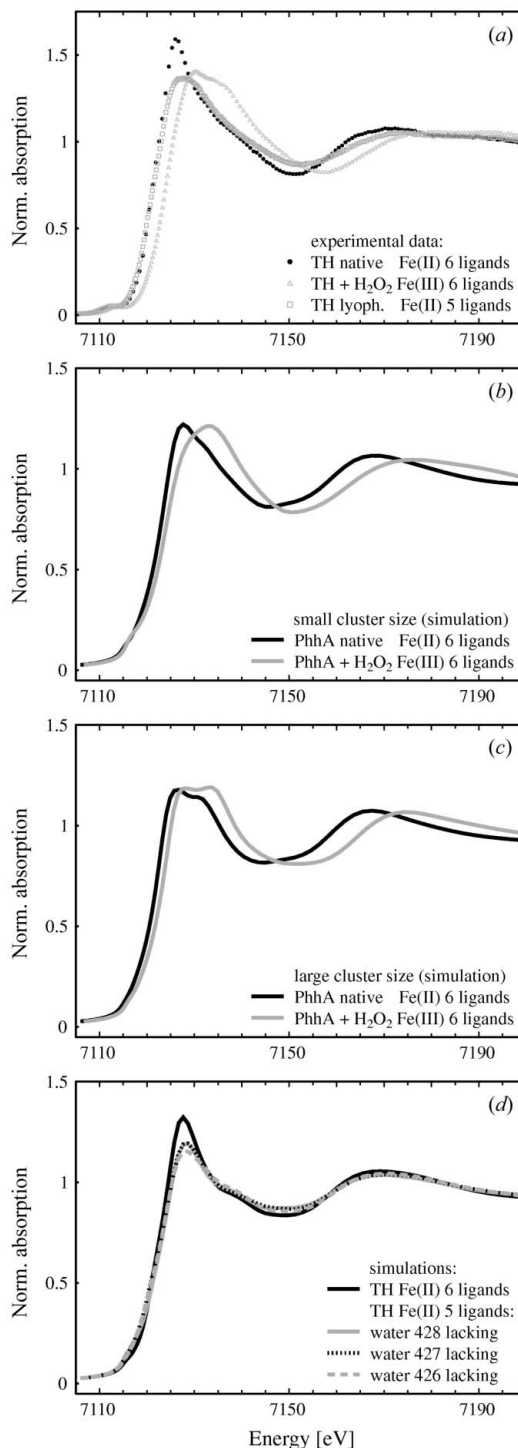


Figure 2

XANES for the 2-His-1-carboxylate motif. (a) Experimental data for human tyrosine hydroxylase in the native, lyophilized native and oxidized state (Meyer-Klaucke *et al.*, 1996; Schünemann *et al.*, 1999). (b) Simulations based on a small sphere for phenylalanine hydroxylases [Fe(II): 4.33 Å/Fe(III): 4.12 Å] and (c) simulations based on a larger sphere [Fe(II): 5.67 Å/Fe(III): 5.38 Å]. (d) Edge-shape simulations for Fe(II) tyrosine hydroxylase with coordination six and five.

et al., 1998). The strongest contributions to the XANES arise from multiple scattering within a residue and from pathways including the central atom. The later contributions are frequently neglected in EXAFS data analysis but play a key role here. Thus it might be possible to generate identical XANES patterns for two different structures, if the ligand–ligand distances of opposite residues remain constant but the metal–ligand distance changes. By adjusting Asp58 (opposite of Asp134) to a ligand–Zn–ligand distance of 4.19 Å, such a case was simulated. The corresponding angle of 172° is close to a linear arrangement, resulting in strong multiple-scattering contributions. The spectra strongly depend on the individual Zn–ligand distance in the case of differing ligands, but change much less for identical ligands (Fig. 4*d*). This limitation should be accounted for whenever XANES is used as a fingerprint.

4. Discussion

FEFF8.10 can qualitatively reproduce the XANES of metallo-enzymes when the coordination is almost symmetric and a well defined structural model is available. The three typical XANES patterns reported for the 2-His-1-carboxylate motif were simulated. New insight into the catalytic mechanism is available on the basis of such calculations, because the multiple scattering within the first shell is a major contribution to the edge shape. Any alteration in this coordination sphere is reflected by the intensity and position of the resonances. Thus, a ligand removed from the first shell can be determined. In the case of the replacement of an atom by a similar ligand, it became clear why little alteration of the edge pattern is observed. The influence of single atoms in the second or third coordination sphere is rather low. Therefore, the edge shapes reported for the binding of the substrate or cofactor do not differ substantially from those of the reference samples. It might be a future option to calculate difference spectra for such cases, but the requirements for sample homogeneity, noise level of the data and accurate energy calibration are high.

For the metallo β -lactamase, the simulations on the DCH site elucidate limitations in XANES analysis: for identical ligands opposite each other, the resulting XANES depends strongly on the ligand–ligand distance and only to a small extent on the metal–ligand

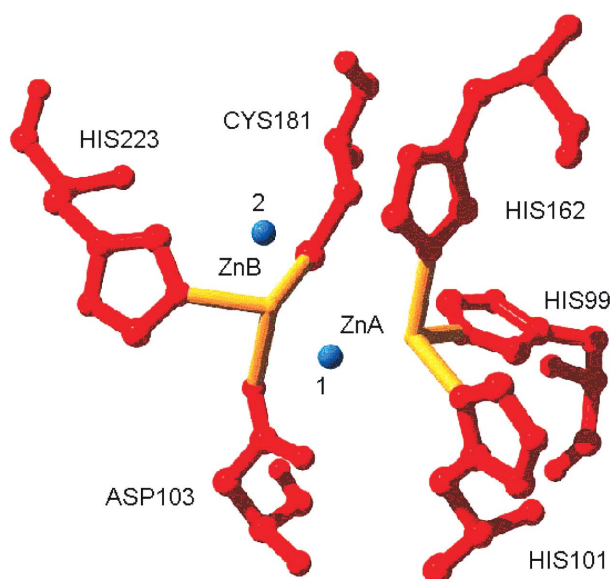


Figure 3
The dinuclear metal site for β -lactamase from *Bacteroides fragilis*.

distances. In contrast, the individual metal–ligand distances play a major role for different ligands. This behaviour defines limits for the use of XANES as a fingerprint in the identification of metal sites. In

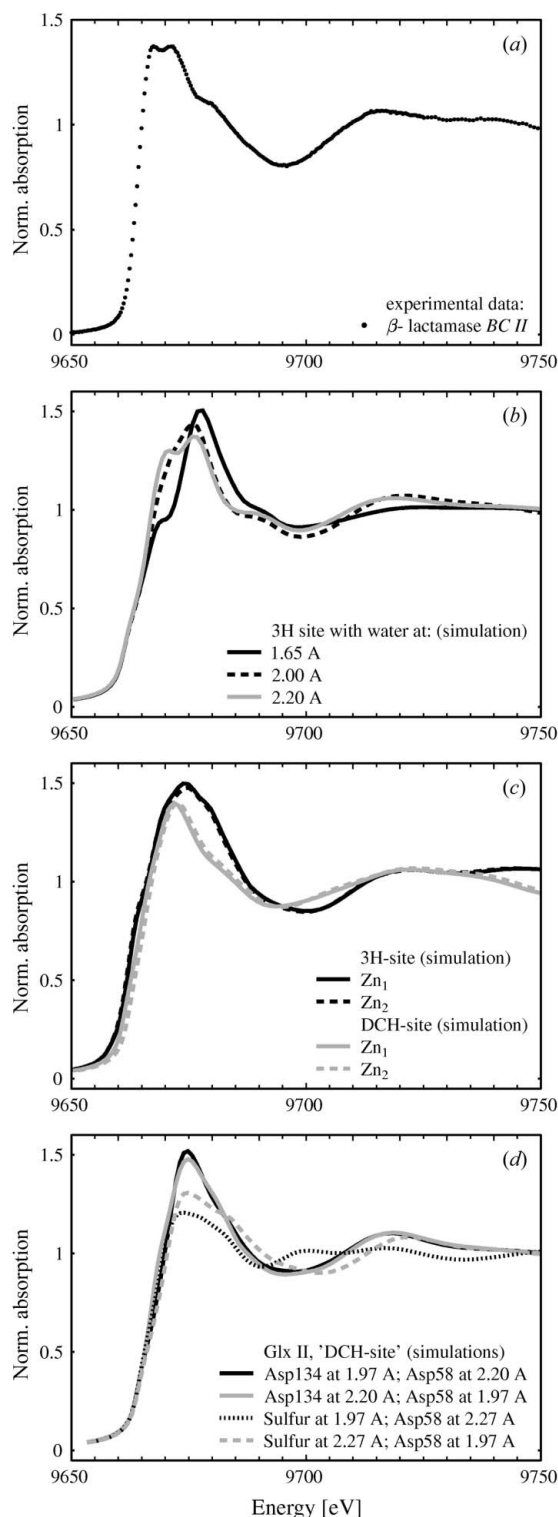


Figure 4
XANES for the Zn β -lactamase motif. (a) Experimental data for *Bacillus cereus* II (Meyer-Klaucke *et al.*, 1999); (b) simulated contribution of the 3H site with three different water distances; (c) individual simulations of the 3H and DCH sites with and without the second Zn ion bound; (d) simulations for the 'DCH site' of glyoxalase II, varying the distances of Asp134 and Asp58 and replacing Asp134 by sulfur.

this context, it is important to note how little the presence of the second metal changes the fingerprint for both β -lactamase sites. This fact explains previous experimental results (Meyer-Klaucke *et al.*, 1999) reporting nearly identical XANES patterns for half- and fully-loaded Zn β -lactamase and supports the model of the distribution of single metal between both sites (De Seny *et al.*, 2001). In this model, the presence of the first metal ion has an inhibitory effect on the binding of the second metal. This is in contrast to previously discussed high- and low-affinity Zn-binding sites (Orellano *et al.*, 1998).

Moreover, the simulations for the 3H site support recent EXAFS results suggesting a short Zn_A–water distance. From the simulations it became clear that a strong distortion of the tetrahedral symmetry has to be expected for this site, which is in contrast to the case of mono-Zn proteins. Their XANES patterns (Kleifeld *et al.*, 2000) resemble the simulations for symmetrical tetrahedral metal coordination.

The individual simulations of both sites are instructive, but the accuracy is at present not sufficient to discuss a superposition of both contributions. Too many limitations are still present in the theory. Apart from the basic problems concerning the potential shape and symmetry, the lack of appropriate static-disorder parameters is also a dilemma. The contributions at distances above 4.4 Å were neglected for the 2-His-1-carboxylate triad, because they introduced additional resonances. The measurements indicate the presence of such contributions at a much lower level. It has to be considered that static disorder for residues not bound to the metal ion can be quite high in proteins. This case, unique for protein samples, has to be introduced into the theory to provide a more powerful tool for research.

Uwe Sauer and Fredrik Ekström (Umeå University, Sweden) are kindly acknowledged for the samples of phenylalanine hydroxylase.

References

- Ankudinov, A. L., Ravel, B., Rehr, J. J. & Conradson, S. D. (1998). *Phys. Rev. B*, **58**, 7565–7576.
- Cameron, A. D., Ridderström, M., Olin, B. & Mannervik, B. (1999). *Structure*, **7**, 1067–1078.
- Carfi, A., Duée, E., Paul-Soto, R., Galleni, M., Frère, J.-M. & Dideberg, O. (1998). *Acta Cryst. D* **54**, 47–57.
- Clark-Baldwin, K., Tieney, D. L., Govindaswamy, N., Gruff, E. S., Kim, C., Berg, J., Koch, S. A. & Penner-Hahn, J. E. (1998). *J. Am. Chem. Soc.* **120**, 8401–8409.
- Della Longa, S., Arcovito, A., Girasole, M., Hazemann, J. L. & Benfatto, M. (2001). *Phys. Rev. Lett.* **87**, 155501.
- De Seny, D., Heinz, U., Wommer, S., Kiefer, M., Meyer-Klaucke, W., Galleni, M., Frère, J.-M., Bauer, R. & Adolph, H.-W. (2001). *J. Biol. Chem.* **276**, 45065–45078.
- Erlandsen, H., Bjørgo, E., Flatmark, T. & Stevens, R. C. (2000). *Biochemistry*, **39**, 2208–2217.
- Erlandsen, H., Flatmark, T., Stevens, R. C. & Hough, E. (1998). *Biochemistry*, **37**, 15638–15646.
- Erlandsen, H., Fusetti, F., Martinez, A., Hough, E., Flatmark, T. & Stevens, R. C. (1997). *Nature Struct. Biol.* **4**, 995–1000.
- Feiters, M. (1990). *Commun. Inorg. Chem.* **11**, 131–174.
- Flatmark, T. & Stevens, R. C. (1999). *Chem. Rev.* **99**, 2137–2160.
- Goodwill, K. E., Sabatier, C., Marks, C., Raag, R., Fitzpatrick, P. F. & Stevens, R. (1997). *Nature Struct. Biol.* **4**, 578–584.
- Hernandez-Valladares, M., Kiefer, M., Heinz, U., Paul-Soto, R., Meyer-Klaucke, W., Nolting, H.-F., Zeppezauer, M., Galleni, M., Frère, J.-M., Rossolini, G.-M., Amicosante, G. & Adolph, H.-W. (2000). *FEBS Letts.* **467**, 221–225.
- Jacquamet, L., Aberdam, D., Adrait, A., Hazemann, J. L., Latour, J.-M. & Michaud-Soret, I. (1998). *Biochemistry*, **37**, 2564–2571.
- Joly, Y. (2001). *Phys. Rev. B*, **63**, 125120.
- Kemsley, J. N., Mitić, N., Loeb Zaleski, K., Caradonna, J. P. & Solomon, E. I. (1999). *J. Am. Chem. Soc.* **121**, 1528–1536.
- Kleifeld, O., Van den Steen, P. E., Frenkel, A., Cheng, F., Jiang, H. L., Opednakker, G. & Sagi, I. (2000). *J. Biol. Chem.* **275**, 34335–34343.
- Loeb, K. E., Westre, T. E., Kappock, T. J., Mitić, N., Glasfeld, E., Caradonna, J. P., Hedman, B., Hodgson, K. O. & Solomon, E. I. (1997). *J. Am. Chem. Soc.* **119**, 1901–1915.
- Meyer-Klaucke, W., Paul Soto, R., Valladares, M. H., Adolph, H.-W., Nolting, H.-F., Frère, J.-M. & Zeppezauer, M. (1999). *J. Synchrotron Rad.* **6**, 400–402.
- Meyer-Klaucke, W., Winkler, H., Schünemann, V., Trautwein, A. X., Nolting, H. F. & Haavik, J. (1996). *Eur. J. Biochem.* **241**, 432–439.
- Mijovilovich, A. & Meyer-Klaucke, W. (2001). *J. Synchrotron Rad.* **8**, 692–694.
- Mijovilovich, A., Sauer, U., Ekström, F. & Meyer-Klaucke, W. (2003). In preparation.
- Orellano, E. G., Girardini, J. E., Cricco, J. A., Ceccarelli, E. A. & Vila, A. J. (1998). *Biochemistry*, **37**, 10173–10180.
- Paul-Soto, R., Bauer, R., Frère, J.-M., Galleni, M., Meyer-Klaucke, W., Nolting, H., Rossolino, G. M., de Seny, D., Hernandez-Valladares, M., Zeppezauer, M. & Adolph, H.-W. (1999). *J. Biol. Chem.* **274**, 13242–13249.
- Penner-Hahn, J. (2000). European Workshop on X-ray Absorption for Biology, Orsay, France, July 3–4. Oral communication.
- Que, L. Jr (2000). *Nature Struct. Biol.* **7**, 182–184.
- Schünemann, V., Meier, C., Meyer-Klaucke, W., Winkler, H., Trautwein, A. X., Knappskog, P. M., Toska, K. & Haavik, J. (1999). *J. Biol. Inorg. Chem.* **4**, 223–231.
- Strange, R. W., Alagna, L., Durham, P. & Hasnain, S. S. (1990). *J. Am. Chem. Soc.* **112**, 4265–4268.